(3) Doi, M.; Edwards, S. F. *J. Chem. Soc., Faraday Trans. 2* **1978**, *74*, 1802.
(4) Gaylord, R. J.; Douglas, J. F. *Polym. Bull.* **1987**, *18*, 347.
(5) Gao, J.; Weiner, J. H. *Macromolecules* **1988**, *22*, 979.
(6) Weiner, J. H.; Gao, J. *Macromolecules* **1989**, *22*, 4544.
(7) See, for example: Gumbrell, S. M.; Mullins, L.; Rivlin, R. S. *Trans. Faraday Soc.* **1953**, *49*, 1495. Allen, G.; Kirkham, M. J.; Padget, J.; Price, C. *Trans. Faraday Soc.* **1971**, *67*, 1278.
(8) Gao, J.; Weiner, J. H. *Macromolecules* **1987**, *20*, 2620.
(9) Note that this is a change in notation from ref 6; there ν represented the number of chains per unit volume.
(10) We make this recasting of eq 3.15 in terms of quantities referring to the dry state in order to conform to usual practice, even though it requires the affine assumption of the first of eq 3.16 whose validity has been placed into question recently; cf. Geissler, E.; et al. *J. Chem. Phys.* **1989**, *90*, 1924. The conclusions regarding the effect of swelling on the predicted strain softening can also be deduced directly from eq 3.15.
(11) To see this result, consider uniaxial extension at constant volume, although the argument is readily extended to general three-dimensional deformations. The partition function Z for the freely jointed, hard-sphere model, or for any model described solely in terms of geometric constraints, takes the form $Z(\lambda, T) = a(T)g(\lambda)$. It then follows that the internal energy $U = kT^2 (\partial/\partial T) \log Z = U(T)$; i.e. the internal energy is independent of the extension λ and the elasticity is purely entropic.

Monte Carlo Simulation of Polymers Confined between Flat Plates

Arun Yethiraj and C. K. Hall*

Department of Chemical Engineering, The North Carolina State University, Raleigh, North Carolina 27695-7905. *Received July 24, 1989*

ABSTRACT: The behavior of polymers (modeled as a pearl necklace of $n = 20$ freely jointed hard spheres) between hard walls is studied by using a canonical ensemble Monte Carlo method. Simulation results for the density profiles and configurational properties are presented for wall separations varying from 4 to 16 hard sphere diameters and for volume fractions of 0.1, 0.2, and 0.3. It is found that the chains are depleted at the wall at the lower density but enhanced at the wall (relative to the center of the pore) at the higher density. The density of end sites of the chain at the wall is higher than it is for middle sites. Near the wall the chains are found to be flattened against the wall; in the large pore the fluid in the middle of the pore is uniform. In the bulk region, the distribution of sites about the center of mass is Gaussian; near the wall it is asymmetric and sharply peaked. In the smallest pore the chains are almost two dimensional. The force on the walls as a function of wall separation is calculated by using a superposition approximation to obtain the density profile for a fluid in small pores from the density profile for a fluid in a large pore at the same chemical potential. At high densities the force is an oscillatory function of wall separation with a period of oscillation of about one bead diameter, but at low densities it is monotonic and attractive.

1. Introduction

In an earlier paper[1] we investigated the behavior of mixtures of short chains (model alkanes) and hard spheres (model methane) confined between plates. In this article we extend the work to pure polymers confined between plates, a problem that is of practical and theoretical interest, which has been the focus of analytical,[2-5] computer simulation,[6-13] and experimental investigations[14,15] in recent years. One objective of this work is to determine if the behavior of long chains is qualitatively different from the behavior we observed earlier for short-chain molecules between plates.[1] Another objective is to gain insight at the molecular level into the behavior of polymers between surfaces.

In this article we use continuous-space Monte Carlo simulation to study the behavior of polymers confined between flat plates. Each polymer molecule is modeled as a pearl necklace of 20 freely jointed hard spheres, long enough to behave like polymer molecules but short enough to allow for intensive computer study. The choice of 20 as a sufficient length for polymeric behavior is supported by recent surface forces apparatus measurements on polybutadiene,[15] which reported a transition from alkane-like to polymer-like behavior at a chain length of $n \geq 20$. The walls of the pore are taken to be hard walls impenetrable to the centers of the sites on the chains. By modeling the walls and segments as hard bodies, we eliminate enthalpic effects and focus instead on the entropic effects associated with chain confinement. We might emphasize that, unlike that of bulk fluids, the structure of confined fluids is sensitive to the attractive part of the interactions, especially at low densities. In other words, enthalpic effects, which we eliminate, can be important in real systems.

The simulations of chains between hard walls are performed by using a modified version of an algorithm developed by Dickman and Hall[9] and later used by Yethiraj and Hall.[1] The wall separation is varied from 4σ to 16σ (where σ is the hard-sphere diameter). Three volume fractions, 0.1, 0.2, and 0.3, are considered. At ambient conditions, the volume fraction of polyethylene is approximately 0.31.[16] We report the density profiles of the fluid, the conformations of the chain in large and small pores, and the force on the walls as a function of the wall separation. We find that the behavior of 20-mers between walls is qualitatively similar to the behavior of short chains that we reported earlier.[1] At low densities, the chains are depleted at the wall relative to the middle; at high densities the chains are enhanced at the wall relative to

0024-9297/90/2223-1865$02.50/0

the middle. Near the wall the chains are flattened like pancakes against the wall; in large pores the fluid in the middle of the pore is essentially uniform. Chains are almost two dimensional in the smallest pore. In the pore center, the distribution of chain sites about the center of mass is Gaussian. Near the wall the distribution is sharply peaked and asymmetric.

To estimate the force on the walls as a function of wall separation we use the superposition approximation used by van Megen and Snook[17] to calculate the density profile for a fluid in a small pore from the density profile of a fluid in a large pore at the same chemical potential. We find that this force is an oscillatory function of the wall separation at high densities but non-oscillatory and attractive at low densities. This is contrary to the experimental observations on polybutadiene melts,[15] where the force was found to be a repulsive and monotonically decaying function of the separation between the walls, but consistent with more recent experimental observations on poly(dimethylsiloxane).[18]

In section 2 we present our Monte Carlo method, in section 3 we discuss density profiles and chain conformations, and in section 4 we discuss the solvation forces between the walls.

2. Simulation Method

Monte Carlo simulations are performed in the canonical ensemble (number of molecules, volume, and temperature constant). The simulation cell is a rectangular parallelepiped bounded on two sides by hard structureless walls. The walls are placed a distance $H\sigma$ apart in the z direction and are assumed to be impenetrable to the centers of the sites (beads) on the chains. Periodic boundary conditions are employed in the directions parallel to the wall, that is, in the x and y directions. In all the simulations, $N = 40$ chains consisting of $n = 20$ tangent hard spheres are used. The periodic length L is adjusted to achieve the desired density. The periodic length varies from 9.34σ (at the highest density and $H = 16$) to 32.36σ (at the lowest density and $H = 4$).

In a straightforward application of the Metropolis algorithm,[19] successive configurations are generated by moving one chain; the move is accepted if the new configuration is free of overlap and rejected otherwise. To generate new configurations we use two types of moves, the translate–jiggle move of Dickman and Hall[9] and the slithering snake (reptation) move.[20] In the translate–jiggle move, the test chain is subjected to a random translation followed by a "jiggling" in which all segments undergo a smaller displacement that is normalized so that all bond lengths are maintained at σ. The magnitudes of the displacements are adjusted so that 30–35% of all these moves are accepted. In the slithering snake move, one of the end beads of the chain is chosen randomly and then removed and replaced randomly at the other end of the chain. Both the moves are believed to sample all of configuration space,[9,10] thus the combination of the two should also. The type of move used at each step is chosen randomly and with equal probability.

The simulation consists of three phases, initial configuration generation, equilibration, and averaging. Table I summarizes the number of moves required for equilibration and averaging for all the simulations performed.

Initial configurations are generated by using a continuous-space analogue of the growth algorithm used in lattice simulations.[6,12] First, N hard spheres are randomly inserted into the simulation cell, and then these spheres are grown into chains. Each cycle consists of two steps:

Table I
Summary of Simulations Performed

	relaxation moves × 10^{-6}			equilibrium moves × 10^{-6}		
η	$H = 4$	$H = 8$	$H = 16$	$H = 4$	$H = 8$	$H = 16$
0.1	2	4	4	10	10	10
0.2	3	5	9	10	11	12
0.3	3	6	24	12	16	53

an attempt to move a randomly chosen chain, followed by an attempt to add a bead to another randomly chosen chain (provided this chain is not already fully grown). The process is continued (regardless of the outcome of each step) until all the chains are fully grown. Growing of an initial configuration (all of which consist of 40 20-mers) requires approximately 31 000 cycles at the highest density and 2250 cycles at the lowest density. In our earlier work[1,9] we generated initial configurations by randomly inserting chains into the simulation cell; we find that growing chains is about 100 times faster.

After the initial configuration is generated, the system is equilibrated to ensure that the measured properties are independent of the initial state. Symmetry of the density profiles about the center of the pore is used to determine if the system is relaxed. In addition the system is assumed to be relaxed only if all the sites have moved at least 2σ from their original position. Typical relaxation times are on the order of 1.5×10^5 to 3.75×10^5 attempted moves per chain.

The density profile is recorded by dividing the region between the walls into a number of equal-sized bins. After a certain number of moves (the number varies between 50 and 100) the number of sites in each bin is recorded. (We call this an "accumulation step".) The density profile is obtained by averaging the number of sites in the bin over the length of the run. Center of mass and individual site profiles are obtained in a similar manner except that bigger bins are required as the number of individual sites and chain centers of mass is smaller than the number of chain sites. We also monitor the mean-square radius of gyration, the mean-square end-to-end distance, and the distribution of sites about the center of mass, as a function of the position of the center of mass. Properties are averaged over 10–50 runs consisting of at least 1 million moves each. The variation of the averages of each of these runs is used to determine the standard deviation errors in the simulation. Errors in the total site density profiles are about 2%. Errors in the center of mass and individual site density profiles are about 5–8%.

Simulations were performed on a Cray X-MP with a CPU time per attempted move of approximately 0.0021 s.

3. Density Profiles and Conformational Properties

The simulations were performed for 20-mers at overall volume fractions of 0.1, 0.2, and 0.3, each at pore widths of $H = 4$, 8, and 16.

This section is subdivided into two parts. In section A we discuss the interplay between packing and entropic effects, and in section B we discuss the conformation of chains in the pore.

A. Entropic/Packing Effects. The density profiles are governed by a competition between entropic and packing effects.[1] The chains near the wall experience a decrease in configurational entropy, which makes the region near the wall entropically unfavorable. On the other hand, the chains near the wall suffer collisions with the chains away from the wall, which tends to move the chains near

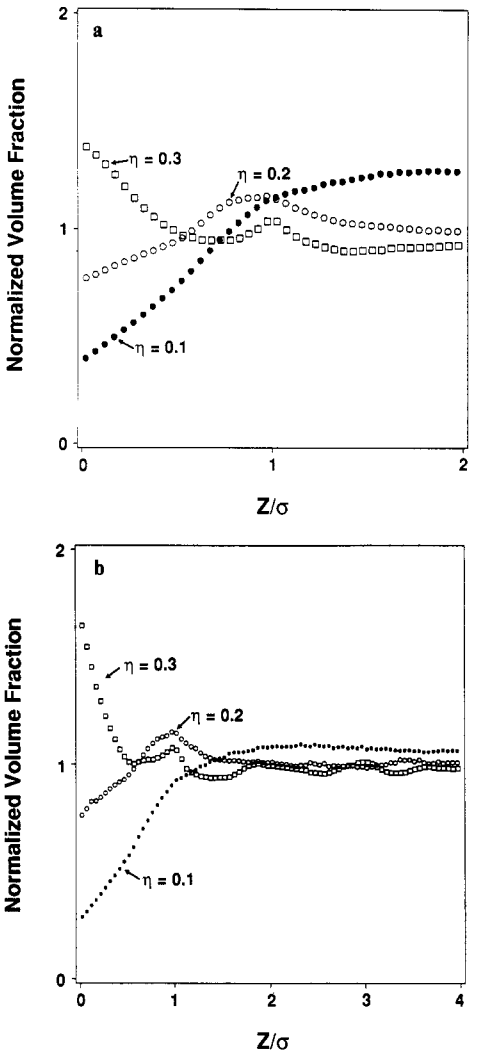

Figure 1. Local density profiles near the wall at (a) $H = 4$ and (b) H = 16.

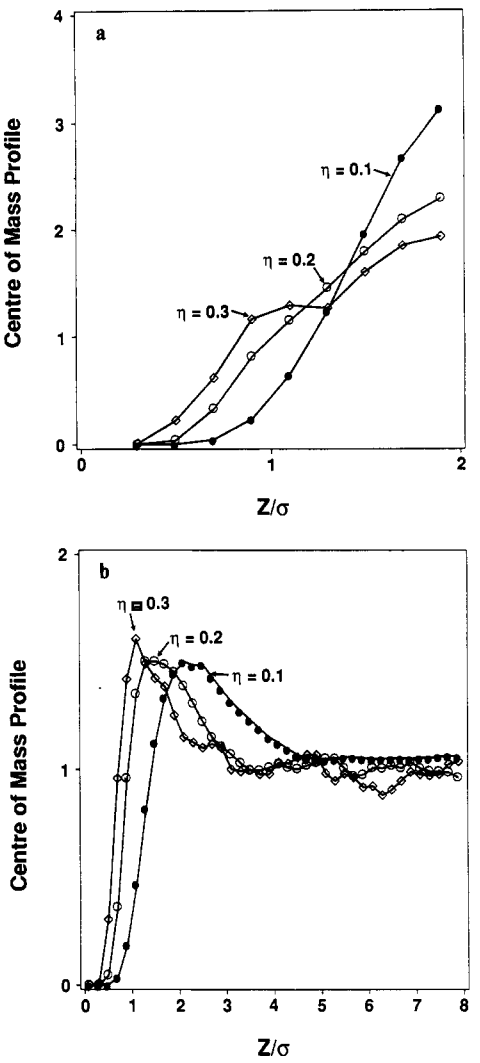

Figure 2. Center of mass profiles at (a) $H = 4$ and (b) $H = 16$.

the wall closer to the wall (packing effect). At low densities entropic effects dominate, while at high densities packing effects dominate.

The competition between entropic and packing effects can be observed in parts a and b of Figure 1, which show the density profiles for volume fractions of 0.1, 0.2, and 0.3 at wall separations of $H = 4$ and $H = 16$, respectively. The ordinate in these figures is the total volume fraction of chains normalized to the average value in the cell. (The profiles for $H = 8$ are very similar to those for $H = 16$ and have therefore been omitted.) At the lowest volume fraction ($\eta = 0.1$) entropic effects are important and we observe a depletion of chain sites near the wall. At the highest volume fraction ($\eta = 0.3$) packing effects are important and we observe an enhancement of chain sites at the wall. The profiles at the higher density are similar to the profiles of hard spheres at a wall and the oscillations are due to the packing of the chains against the wall. At the intermediate volume fraction, both entropic and packing effects are equally important. As a result, the chains are depleted at the wall, but the profile is oscillatory. The profiles are flat in the middle of the large pore (Figure 1b) where the fluid does not feel the walls; in the small pore (Figure 1a) the profiles are never flat because the fluid feels the walls everywhere in the pore. These enhancement/depletion effects have been previously reported in simulations of short chains.[1,9] The packing of chains at high densities has been seen in the simulations of Kumar et al.[10] and Bitsanis.[11] The packing effect cannot be observed in lattice simulations[12,13] because the segments of the chain are restricted to the sites of a regular lattice. However, lattice simulations[6,7] do show the transition from depletion at the wall to enhancement at the wall as the volume fraction is increased.

The entropic/packing effects are observed at the molecular level as well as the site level described above. Parts a and b of Figure 2 depict center of mass profiles at $H = 4$ and $H = 16$, respectively. The center of mass profiles are normalized to the average center of mass density in the cell. Near the wall the center of mass density is low because for a chain center of mass to approach the wall the chain has to be in a severely flattened (entropically unfavorable) conformation. As the density is increased, however, the packing of chains at the wall pushes the chain centers nearer the wall. At $H = 4$ the chain centers much prefer the middle of the pore to the region near the wall; at $H = 16$ the profiles go through a maximum at about 1–3σ from the wall and are level in the middle of the pore where the fluid is isotropic. At the lowest density the maximum in the profile is at a distance approximately equal to the root-mean-square radius of gyration, R_g^0, of bulk chains at this density. This can be explained if we model the chains as large hard spheres of radius R_g^0,[1] an approximation that is not too bad at low densities. One would expect a maximum in the profile at the distance of closest approach of the big spheres,

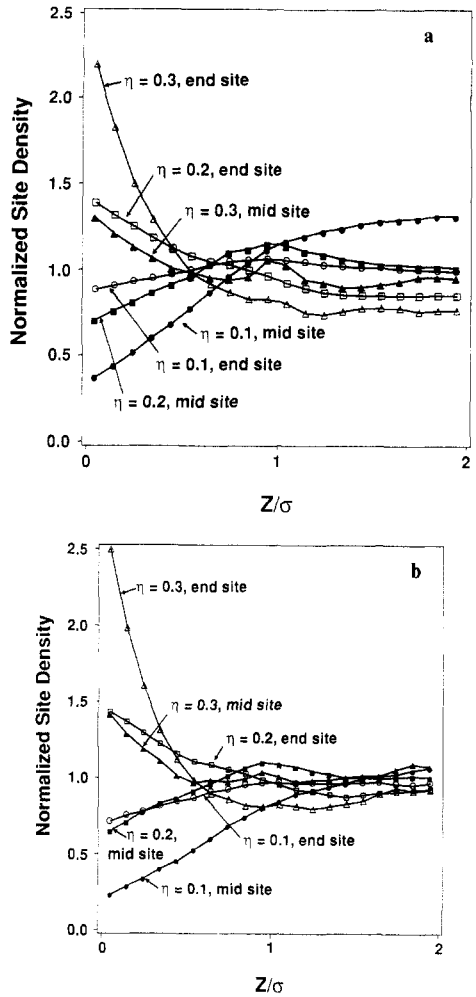

Figure 3. Individual site profiles at (a) $H = 4$ and (b) $H = 16$.

i.e., at $z/\sigma \approx R_g^0$, and this is what is observed in the chain simulations at low density. At higher densities the chains interpenetrate each other so the "effective" large hard sphere model is no longer appropriate. The packing of the chains causes the maximum in the profile to be pushed toward the wall as the density is increased. The profiles in Figure 2 are similar to the profiles of 8-mers reported in an earlier paper at similar densities[1] and are consistent with the simulations of others.[6,7,10,12,13] We do not believe the oscillations in the center of mass profile at the highest density to be real; the error bars are about as large as the amplitude of these oscillations. All our other data support the conclusion that the fluid in the middle of the pore is isotropic.

We also investigate the effect of density on the profiles of the individual sites along the chain. Parts a and b of Figure 3 show the individual site profiles for an end site and a middle site at $H = 4$ and 16, respectively. The profiles are normalized to the average volume fraction of the sites in the pore. The competition between entropic and packing effects is evident here. At the wall, both the end sites and the middle sites are depleted for $\eta = 0.1$, the end sites are enhanced but the middle sites are depleted for $\eta = 0.2$, and both the end sites and the middle sites are enhanced for $\eta = 0.3$. In all cases, the density of end sites at the wall is higher than that of the middle sites. This is because it is entropically less restrictive to expose a chain end to the hard wall than it is to expose the middle of the chain to the hard wall with the ends sticking out on either side.[21] The depletion of end sites relative to the middle sites has been observed previously.[1,6,7,10,11] In the larger pore ($H = 16$) the density of all the individual sites along the chain is about equal in the middle of the pore, suggesting that the fluid is isotropic there. This is not the case in the small pore ($H = 4$).

B. Chain Conformations. In order to study the conformations of chains it is convenient to define the ith component ($i = x, y, z$) of the mean-square radius of gyration, $R_{g,i}^2$, and the mean-square end-to-end distance, R_i^2, as

$$R_{g,i}^2 = \left\langle \frac{1}{n}\sum_{j=1}^{n}(r_{j,i} - r_{cm,i})^2 \right\rangle \quad (1)$$

and

$$R_i^2 = \langle (r_{n,i} - r_{1,i})^2 \rangle \quad (2)$$

respectively. In the above, $r_{j,i}$ is the ith component of the position of the jth site on the chain and $r_{cm,i}$ is the ith component of the position of the center of mass. Recall that the z direction is perpendicular to the walls, and the x and y directions are parallel to the waters. If $R_{g,z}^2$ is smaller than $R_{g,x}^2$ the chains are more compressed in the z direction than they are in the x direction.

We monitor the $R_{g,i}^2$ and R_i^2 components as a function of the position of the center of mass by recording the average square radius of gyration and square end-to-end distance of the chains in each center of mass bin. The components of the mean-square radius of gyration are plotted as a function of the position of the center of mass in parts a, b, and c of Figure 4, which are at $H = 4$, 8, and 16, respectively. By symmetry the x and y components should be equal (we used this symmetry condition to check our results) and we therefore plot the average of the x and y values as the parallel component. The plots for the mean-square end-to-end distance show similar trends and have therefore been omitted. Values of R^2 ($\equiv \sum R_i^2$) and R_g^2 ($\equiv \sum R_{g,i}^2$) in the middle of the large pore ($H = 16$) are summarized in Table II.

We find that near the walls the chains are severely flattened in the direction perpendicular to the walls. Near the wall, the parallel component of the radius of gyration is much larger than the perpendicular component for all pore widths and densities (see Figure 4). This flattening of chains near the wall has been observed before.[1,6,7,11-13] At $H = 16$, the components are equal in the middle of the pore where the fluid is bulklike, but in the smaller pores ($H = 4$ and $H = 8$), the fluid is not isotropic anywhere. Figure 4 shows that the flattening of the chains becomes less pronounced as the density is increased. This is because the chains interpenetrate each other at high densities, resulting in a decrease in the size of the chain.

The decrease in chain size with increasing density in bulk fluids is predicted by scaling theories.[22] For semidilute solutions, scaling theories predict that $R^2 \sim \eta^{-0.25}$. We compare our simulations to these theories by using average R^2 values in the middle of the large pore and by plotting ln $(R^2/6)$ versus ln η. The slope of this curve in the semidilute regime will give up the exponent of η. Figure 5 is a plot of ln $(R^2/6)$ versus ln η. (Also included are some preliminary results of simulations that will be reported elsewhere.) The transition from the dilute to semidilute regime occurs at a volume fraction $\eta^* \approx 6n/(\pi R^3)$, which is at about $\eta^* \approx 0.16$. We therefore fit a least-squares line to the last four points; the line has a slope of −0.224, which is close to the scaling theory prediction.

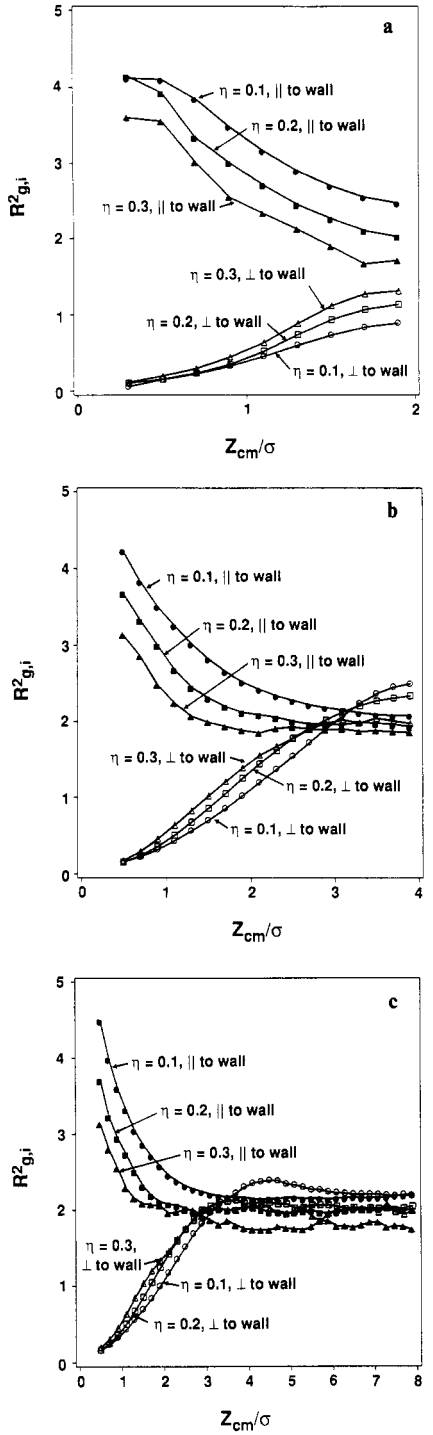

Figure 4. Mean-square radius of gyration profiles at (a) H = 4, (b) H = 8, and (c) H = 16.

Table II
R^2 and R_g^2 in the Bulk

η	R_g^2	R^2
0.1	6.56 ± 0.03	41.49 ± 0.35
0.2	6.05 ± 0.06	37.37 ± 0.64
0.3	5.65 ± 0.10	34.74 ± 0.95

We also monitor the distribution of chain sites about the center of mass. For every chain in each center of mass bin, the distance of each site from the center of mass in the x, y, and z direction was calculated. Histograms were maintained in the x, y, and z directions of the number of sites belonging to a chain that were at various distances less than half a chain length from the center of mass. We thus obtained the average distribution of sites about the center of mass in the x, y, and z directions as a function of the position of the center of mass. These are plotted in Figures 6 and 7. In the figures, $f(u)$ ($u = x, y, z$) is the normalized probability density that a site will be found at a distance $u - u_{cm}$ from the center of mass. The distribution of sites in the x and y directions was found to be almost equal, and the average value is plotted as $f(x)$. $f(z)$ is the distribution of sites in the z direction.

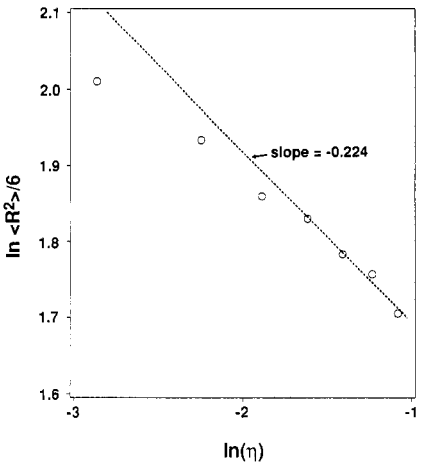

Figure 5. Variation of mean-square end-to-end distance with density. The line is a least-squares fit to the last four points.

We can compare the site distributions observed to a Gaussian site distribution. Strictly, the distribution of segments about the center of mass is Gaussian only as $n \rightarrow \infty$;[23] however, we shall see that this is a very reasonable approximation in the bulk region of our system. For a Gaussian chain, if we assume the site distributions in the x, y, and z directions are independent of each other, we have

$$f(x) = \left(\frac{3}{2\pi R_g^2}\right)^{1/2} \exp\left(-\frac{3x^2}{2R_g^2}\right) \tag{3}$$

for a chain in three dimensions and

$$f(x) = \left(\frac{1}{\pi R_g^2}\right)^{1/2} \exp\left(-\frac{x^2}{R_g^2}\right) \tag{4}$$

for a chain in two dimensions.

In the large pore the distribution of sites about the center of mass depends strongly on the distance of the center of mass from the wall. The distribution in the direction perpendicular to the wall (the z direction) is Gaussian in the middle of the pore but is asymmetric and sharply peaked near the wall. Parts a and b of Figure 6 show the distribution of sites about the center of mass in the direction perpendicular to the walls at H = 16 and for η = 0.1 and 0.3, respectively. Three distributions are shown in the figure: a distribution for which $0 < z_{cm} < 1$, a distribution for which $1 < z_{cm} < 2$, and a distribution in the pore center. The wall is to the left of the curves in the figures. Also shown is the Gaussian distribution given by eq 4, which uses bulk R_g^2 values obtained from our simulations. In the middle of the pore the site distribution is Gaussian, while near the wall the distribution is sharply peaked and asymmetric, being more compressed in the direction toward the wall than the other. This asymmetry in the distribution near the wall is more marked at the higher density (Figure 6b) than at the lower density (Figure 6a). At the higher density (Figure 6b) the distribution of sites shows more than one maximum, which roughly correspond to the maxima in the total den-

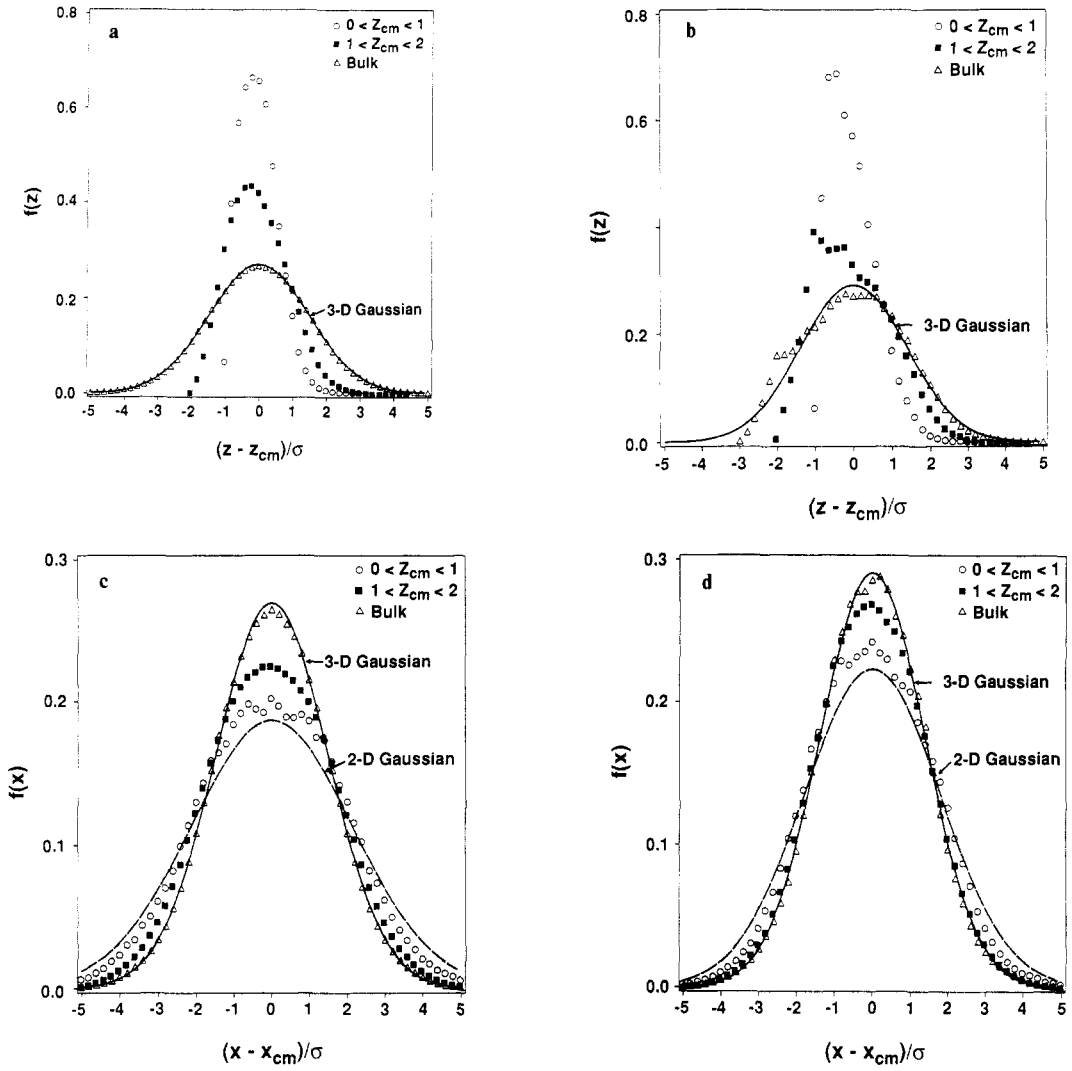

Figure 6. Distribution of sites about the center of mass in a large pore: (a) $\eta = 0.1$, perpendicular to the wall; (b) $\eta = 0.3$, perpendicular to the wall; (c) $\eta = 0.1$, parallel to the wall; (d) $\eta = 0.3$, parallel to the wall.

sity profile (see Figure 1b). The coarseness of the center of mass bins used in these measurements, however, prevents us from drawing any further conclusions on the relationship between these maxima. The site distribution in the direction parallel to the walls is always bell shaped. However, near the wall the curves decay much slower than in the bulk. This can be seen in parts c and d of Figure 6, which show the site distribution in the direction parallel to the walls at $H = 16$ and for $\eta = 0.1$ and 0.3, respectively. Again, three distributions are shown in the figure: a distribution for which $0 < z_{cm} < 1$, a distribution for which $1 < z_{cm} < 2$, and a distribution in the pore center. The longer range of the distributions for chain centers near the wall is a consequence of the chains being flattened near the wall. Also plotted in the figure is the Gaussian distribution for two- and three-dimensional chains, which use bulk R_g^2 values obtained from our simulations. For chains near the wall, the distribution is closer to the two-dimensional Gaussian than the three-dimensional Gaussian. In the bulk, the fluid is isotropic and the site distribution is the same in both the parallel and perpendicular directions.

In the small pore ($H = 4$) the chains are severely flattened. Parts a and b of Figure 7 show the site distribution profiles at $H = 4$ in both the z and x directions, for $\eta = 0.1$ and 0.3, respectively. The distribution in the z direction is far from being a three-dimensional Gaussian. This is particularly evident in Figure 7b. Similar behavior has also been observed in the simulations of Bitsanis.[11] In Figure 7a we see that the distribution in the parallel direction is almost satisfied by the Gaussian for two-dimensional chains. Clearly, the chains are almost two dimensional in the small pore. At the higher density, the chains interpenetrate and are therefore not two dimensional. Again, the distribution at the higher density displays maxima that roughly correspond to the maxima in the total site density profile (see Figure 1a).

4. Solvation Forces

Israelachvili and co-workers[14,15] have experimentally measured the force on two surfaces due to a chainlike fluid confined between them. Using their surface force measurement apparatus they measured the force between two crossed cylinders that were immersed in the fluid. Since these were equilibrium measurements, the fluid between the surfaces was in chemical equilibrium with the surrounding fluid. The statistical ensemble that corresponds to the physical situation above is the grand canonical ensemble in which the chemical potential, volume, and temperature are constant. In grand canonical ensemble simulations, the force as a function of wall separation at fixed chemical potential can be calculated directly from the density profile of the fluid at various values of the wall separation.[17]

Simulation of chains in the grand canonical ensemble is notoriously difficult, because, in addition to moving

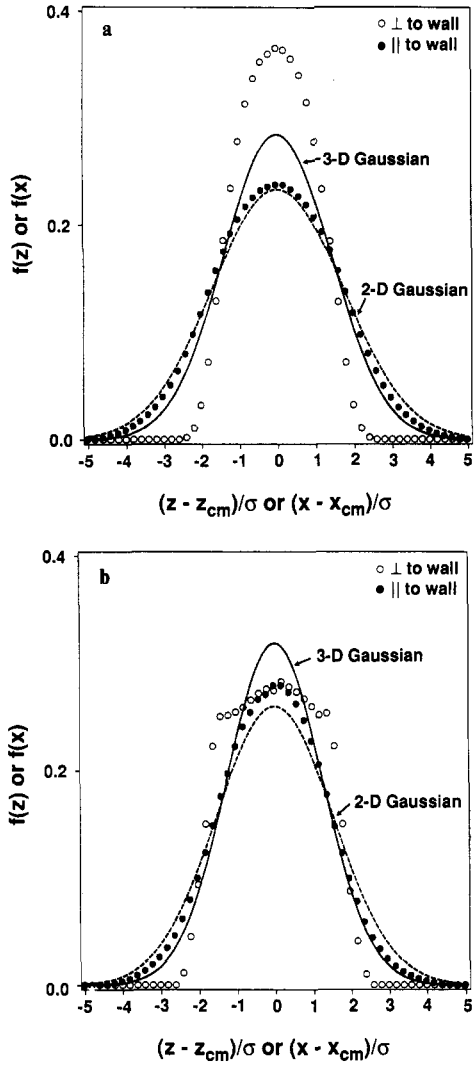

Figure 7. Distribution of sites about the center of mass in a small pore for (a) $\eta = 0.1$ and (b) $\eta = 0.3$.

the molecules, successive states are created by randomly changing the number of molecules in the system with a probability related to the chemical potential. This requires the random insertion of molecules into the fluid. Since successful insertion of chains into a chain fluid without overlap is unlikely, the method is not used. The problem of performing grand canonical ensemble simulations to calculate the forces between fluid-containing walls as a function of their separation was circumvented by van Megen and Snook.[17] They invoked a superposition approximation to estimate the density profile of a fluid in a small pore at a fixed chemical potential given knowledge of the density profile of the fluid at a single wall at the same chemical potential.

In the superposition approximation the density profile, $\rho_h(z)$, in a pore of width h is given by[17]

$$\rho_h(z) = \rho_1(z) + \rho_1(h - z) - \rho_b \tag{5}$$

where z is the distance along the pore (whose walls are at $z = 0$ and $z = h$), $\rho_1(z)$ is the density profile of the fluid at a single wall (or in very large pore), and ρ_b is the bulk density of the fluid at a single wall. van Megen and Snook's force calculations using the superposition approximation[17] showed qualitative agreement with force calculations using grand canonical ensemble simulations performed later by the same authors.[24] The canonical ensemble simulations were at a higher density thus ruling out an exact comparison.

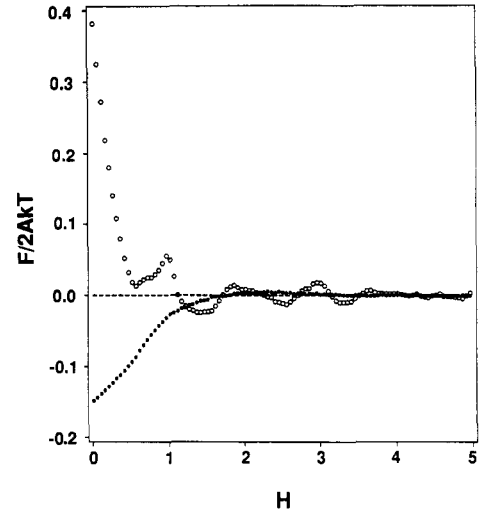

Figure 8. Solvation force as a function of wall separation: $\eta = 0.1$ (filled circles) and $\eta = 0.3$ (open circles).

For a chain fluid between hard walls at a separation h, the force is simply related to the density at the wall[9] by

$$F_h/2AkT = n\rho(0) \tag{6}$$

where F_h/A is the force per unit area on a single wall,[25] $\rho(0)$ is the chain density, and n is the chain length. The solvation force per unit area is given by $F_s = F_h - F_1$[17] where F_1 is the force per unit area when the walls are infinitely far apart. From the superposition approximation (eq 5) the force on the walls as a function of the wall separation is found to be

$$F_s/2AkT = n(\rho_1(h) - \rho_b) \tag{7}$$

Note that we cannot use *our* simulations at $H = 4$, 8, and 16 to obtain the force as a function of wall separation because these are at different chemical potentials. We assume, however, that $H = 16$ adequately represents the case where the walls are infinitely far apart, and we use the profiles in Figure 1b to obtain $\rho_1(z)$.

We plot the force (given by the left-hand side of eq 7) as a function of wall separation in Figure 8 for $\eta = 0.1$ and 0.3. We find that at liquidlike densities ($\eta = 0.3$) the solvation force is repulsive at low wall separations and is an oscillatory function of wall separation with a period of oscillation of approximately one bead diameter. This is consistent with the experimental observations of Christenson et al.[14] on linear alkanes with $n \leq 16$. At gaslike densities ($\eta = 0.1$) the solvation force is attractive and monotonic as predicted by some mean-field theories.[15]

Israelachvili et al.,[15] in their work on polybutadiene melts, observed no oscillations but rather an exponentially decaying repulsion. They observed this "polymer-like" force variation for polymers with $n \geq 20$. The disagreement between our simulations and these force measurements could be due to one of the following: (1) our model is extremely simple and does not consider dispersion and other forces between the molecules, (2) the superposition approximation we use may not be very good for chains, and (3) there might be branching in the polymers used in the experimental measurements. We can argue that our choice of intermolecular potential and the superposition approximation should not affect the force law qualitatively. The oscillatory force law is a consequence of the packing of the molecules, a phenomenon that is well described by the hard potential; the super-

position approximation is not expected to introduce qualitative errors. Branching in the chains, however, should have a marked effect. Branched chains cannot pack as efficiently as linear chains, and in a melt they are likely to be more entangled than linear chains. We therefore believe that branching in the polymer is the most likely reason for the discrepancy between simulations and experiment. Israelachvili et al.[15] suggested that the monotonic force law they observed was due to the branching in their chains. They did not, however, measure the degree of branching in their polymer samples. They further stated that similar force laws should also be observed for linear chains, except that the chain length where the transition from oscillatory to monotonic force laws occurs might be higher. As mentioned earlier, the oscillatory force law is a consequence of the packing of the molecules, an effect that is observed in simulations of long (100 bead) linear chains between walls.[10] We therefore conclude that branching in the chain molecules is most likely to be the cause of the monotonic force law observed in experiments. A more recent investigation[18] suggests that the monotonic force law observed by Israelachvilli et al.[15] is not an equilibrium phenomenon but rather a viscous drag effect. The new measurements (on poly(dimethylsiloxane)) show an oscillatory force behavior at small separation of the surfaces. The effect of branching on the force law, however, has not been investigated.

5. Conclusions

Canonical ensemble Monte Carlo simulations are performed for a polymer fluid between walls. The polymer chains are modeled as a pearl necklace of 20 freely jointed hard spheres. The qualitative features of the density profiles are similar to those observed in our earlier simulations of short chains.[1] It is found that the volume fraction of the chains is lower at the wall than in the middle of the pore for low volume fractions but higher at the wall than in the middle for high volume fractions. This behavior can be explained as a superposition of two factors: entropic effects and packing effects. We show that in large pores, the fluid is isotropic in the middle of the pore.

We see that at the walls of the pore the density of the end sites along the chains is higher than that of the middle sites. Chains near the wall are flattened, though very few chain centers of mass are found near the wall. In small pores the chains are flattened in a direction parallel to the wall and form a nearly two-dimensional structure. In larger pores, chains near the wall are flattened, but the fluid is isotropic and "bulklike" in the middle of the pore. The transition from the flattened structure near the wall to the bulklike behavior in the middle is gradual.

In the middle of the large pore, the distribution of the chain sites about the center of mass is Gaussian. Near the wall, however, the site distribution in the direction perpendicular to the wall is peaked and asymmetric, decaying faster in the direction toward the wall than in the direction away from the wall. In the small pore, the site distribution in the direction parallel to the wall is well described by a Gaussian for two-dimensional chains, suggesting that the chains are two dimensional in the smallest pore.

We use a superposition approximation to calculate the force on the walls as a function of wall separation and find that at liquidlike densities the force is oscillatory with a period of oscillation of about one bead diameter. This is consistent with the experiments on alkanes performed by Christenson et al.[14] and experiments on poly(dimethylsiloxane) performed by Horn et al.[18] but not with the experiments on polybutadiene melts performed by Isrealachvili et al.[15] At gaslike densities the force as a function of wall separation is monotonic and attractive.

We might emphasize that, unlike bulk fluids, the structure of confined fluids is sensitive to the attractive part of the interactions. Therefore these simulations are not expected to adequately describe real systems except at high densities, when packing effects dominate the structure.

Acknowledgment. This study was supported by the Gas Research Institute under Grant 5082-260-724. We gratefully acknowledge Cray Research Inc. for generously allowing us to use their X-MP computer at Mendota Heights, MN. We would also like to thank Dr. R. Czech for helpful discussions and Dr. I. Bitsanis and Prof. D. N. Theodorou for providing results of their simulations prior to publication.

References and Notes

(1) Yethiraj, A.; Hall, C. K. *J. Chem. Phys.* **1989**, *91*, 4827.
(2) Daoud, M.; de Gennes, P.-G. *J. Phys. (Paris)* **1977**, *38*, 85.
(3) DiMarzio, E. A.; Rubin, R. J. *J. Chem. Phys.* **1971**, *55*, 4318.
(4) Eisenriegler, E.; Kremer, K.; Binder, K. *J. Chem. Phys.* **1982**, *77*, 6296.
(5) Chandler, D.; McCoy, J. D.; Singer, S. J. *J. Chem. Phys.* **1986**, *85*, 5971.
(6) Madden, W. G. *J. Chem. Phys.* **1987**, *87*, 1405.
(7) Madden, W. G. *J. Chem. Phys.* **1988**, *88*, 3934.
(8) Olaj, O. A.; Lautschbauer, W.; Pelinka, K. H. *Chemie-Kunstoffe Aktuelle* **1978**, *32*, 199.
(9) Dickman, R.; Hall, C. K. *J. Chem. Phys.* **1988**, *89*, 3168.
(10) Kumar, S. K.; Vacatello, M.; Yoon, D. Y. *J. Chem. Phys.* **1988**, *89*, 5206.
(11) Bitsanis, I. Personal communication.
(12) Ten Brinke, G.; Ausserre, D.; Hadziioannou, G. *J. Chem. Phys.* **1988**, *89*, 4374.
(13) Mansfield, K. F.; Theodorou, D. N. *Macromolecules*, in press.
(14) Christenson, H. K.; Gruen, D. W. R.; Israelachvili, J. N. *J. Chem. Phys.* **1987**, *87*, 1834.
(15) Israelachvili, J. N.; Kott, S. J. *J. Chem. Phys.* **1988**, *88*, 7162.
(16) Van Krevelen, D. W.; Hoftyzer, P. J. *Properties of Polymers: Their Estimation and Correlation with Chemical Structure*, 2nd ed.; Elsevier: Amsterdam, 1976.
(17) van Megen, W.; Snook, I. K. *J. Chem. Soc., Faraday Trans. 2* **1979**, *75*, 1095.
(18) Horn, R. G.; Hirz, S. J.; Hadziioannou, G.; Frank, C. W.; Catala, J. M. *J. Chem. Phys.* **1989**, *90*, 6767.
(19) Metropolis, N.; Rosenbluth, A. W.; Rosenbluth, M. N.; Teller, A. H.; Teller, E. *J. Chem. Phys.* **1953**, *21*, 1087.
(20) Wall, F. T.; Mandel, F. *J. Chem. Phys.* **1975**, *63*, 4592.
(21) DiMarzio, E. A. Personal communication.
(22) Kosmas, M. K.; Freed, K. F. *J. Chem. Phys.* **1978**, *69*, 3647.
(23) Tompa, H. *Polymer Solutions*; Butterworth Scientific Publications: London, 1956; p 243.
(24) Snook, I. K.; van Megen, W. *J. Chem. Phys.* **1980**, *72*, 2907.
(25) The 2 appears in the denominator of eq 6 because A is defined as the area on a single wall. As there are two walls, the force is given by $F = P(2A)$, where P is the pressure.